Nonlinear Dyn (2012) 67:755–765
DOI 10.1007/s11071-011-0024-4

ORIGINAL PAPER

Periodic orbits, basins of attraction and chaotic beats in two coupled Kerr oscillators

I. Śliwa · K. Grygiel

Received: 19 November 2010 / Accepted: 13 March 2011 / Published online: 5 April 2011

Abstract Kerr oscillators are model systems which have practical applications in nonlinear optics. Optical Kerr effect, i.e., interaction of optical waves with nonlinear medium with polarizability $\chi^{(3)}$ is the basic phenomenon needed to explain, for example, the process of light transmission in fibers and optical couplers. In this paper, we analyze the two Kerr oscillators coupler and we show that there is a possibility to control the dynamics of this system, especially by switching its dynamics from periodic to chaotic motion and vice versa. Moreover, the switching between two different stable periodic states is investigated. The stability of the system is described by the so-called maps of Lyapunov exponents in parametric spaces. Comparison of basins of attractions between two Kerr couplers and a single Kerr system is also presented.

Keywords Kerr effect · Kerr couplers · Lyapunov exponents · Basins of attractions · Control of system dynamics · Chaotic beats

I. Śliwa
Theory of Nanostructures Laboratory, Institute of Molecular Physics, Polish Academy of Sciences, ul. M. Smoluchowskiego 17, 60-179 Poznań, Poland
e-mail: izasliwa@ifmpan.poznan.pl

K. Grygiel (✉)
Nonlinear Optics Division, Department of Physics, A. Mickiewicz University, ul. Umultowska 85, 61-614 Poznań, Poland
e-mail: grygielk@amu.edu.pl

1 Introduction

One of the best known and most intensively studied optical models is an oscillator with Kerr nonlinearity. Different kinds of anharmonic Kerr oscillators have also been used to study classical and quantum chaos [1–5]. Mutually coupled Kerr oscillators can be successfully used for a study of couplers, the systems consisting of a pair of coupled Kerr fibers. The first two-mode Kerr coupler has been proposed by Jensen [6] and investigated in depth in [6, 7]. Kerr couplers affected by quantization can exhibit various quantum properties such as squeezing of vacuum fluctuations, sub-Poissonian statistics, collapses, and revivals [8, 9].

In the last two decades since the publication of the paper by Pecora and Carroll [10], the phenomenon of synchronization in systems of the coupled oscillators has become a subject of comprehensive investigation. The problem of synchronization of two linearly coupled Kerr oscillators has been studied in [11] and the possibility of synchronization of chaotic motion was proved numerically. Moreover, the case of synchronization of two kinds of Kerr couplers having a structure of low-dimensional chains (ring and open) has been analyzed [12].

This paper is an attempt at using the modern tools of nonlinear science for numerical investigation of dynamics of a system made of two coupled Kerr oscillators.

In Sect. 2, the basic equation of motion for the single Kerr oscillator is introduced. Simple periodic solutions of equations of motions have been found and the dynamics of the system as well as basins of attraction for such solutions are investigated. Moreover, we calculate the Lyapunov maps for the single Kerr oscillator with external periodic as well as modulated fields. The second case of the external field is used to generate the so-called chaotic beats. In Sect. 3, our single Kerr system analysis is extended over the case of two coupled Kerr subsystems with nonlinear coupling. We find the analytic periodic solutions of such a system. Lyapunov maps and the basins of attraction for this system are helpful tools in analysis of properties of these system. We find that it is possible to change the periodic states of one subsystem by changing the initial conditions of the other subsystem (switching the periodic dynamics). Moreover, it is proved that coupled Kerr subsystems are able to generate of chaotic beats.

2 The single Kerr oscillator

2.1 Equations of motion

We study the dynamical system described by the following Hamiltonian:

$$H = H_0 + H_1, \tag{1}$$

where

$$H_0 = \omega a^* a + \frac{1}{2}\epsilon a^{*2} a^2, \tag{2}$$

$$H_1 = iF\left(a^* e^{-i\Omega_p t} - a e^{i\Omega_p t}\right). \tag{3}$$

The Hamiltonian H_0 represents the so-called Kerr oscillator (if $\epsilon = 0$, then H_0 refers to the harmonic oscillator), whereas the Hamiltonian H_1 describes the interaction of the Kerr oscillator with the periodic external field. The quantities a and a^* are complex dynamical variables describing the amplitudes, ω denotes the frequency of the free vibrations of the harmonic oscillator—basic frequency, ϵ is the parameter describing the Kerr nonlinearity in the system (this is the nonlinearity of the third order), and F is the external field amplitude at the frequency Ω_p.

The equation of motion for variable a has the form:

$$\frac{da}{dt} = -i\omega a - i\epsilon a^* a^2 + F e^{-i\Omega_p t} - \gamma a. \tag{4}$$

The term $-\gamma a$—added on phenomenological grounds —describes the mechanism of loss with the damping constant γ. All the parameters, that is ω, ϵ, F, Ω_p, and γ are taken to be real. The equation of motion for a^* is simply a complex conjugation of (4).

In the autonomous and conservative case, that is when $\gamma = F = 0$, the solution of (4) has a well-known form:

$$a(t) = a_0 e^{-i(\omega + \epsilon a_0^* a_0)t}, \tag{5}$$

where $a(t)\,|_{t=0} = a_0$ is the initial condition.

In the nonautonomous case of (4), we can find the periodic solution:

$$a(t) = x e^{-i(\omega + \epsilon x^* x)t}, \tag{6}$$

that is in the form of the solution of the autonomous one. Function (6) satisfies the equation of motion (4) provided that $x = F/\gamma$. As a result, the periodic solution of (4) has the form:

$$a(t) = \frac{F}{\gamma} e^{-i(\omega + \epsilon \frac{F^2}{\gamma^2})t}. \tag{7}$$

Formally, the function in the form of (7) is the solution of the differential equation (4) only if two condition are fulfilled: (A) $\Omega_p = \omega + \epsilon \frac{F^2}{\gamma^2}$, and (B) the initial condition has the form $a(0) \equiv a_0 = F/\gamma$. In other words, the periodic solution (7) is correct only for special choice of the set of parameters $\omega, \Omega_p, F, \gamma$. Finally, it is worth noting that in our nonautonomous case the period of solution (7) depends on the initial condition which results from condition (B). In the phase plane $(\mathrm{Re}\, a, \mathrm{Im}\, a)$, the periodic solution (7) satisfies the phase equation (circle):

$$(\mathrm{Re}\, a)^2 + (\mathrm{Im}\, a)^2 = F^2/\gamma^2 \tag{8}$$

for any values of frequency ω.

It should be emphasized that the method presented here is useful to find only the one periodic solution for a given set of the system parameters. Generally, the (4) have up to three (not only periodic) solutions.

2.2 The dynamics of the system in the phase space

As a numerical example, let us consider the dynamics of a system described by (4), if $\omega = 1$, $\gamma = 0.5$,

$\epsilon = 0.01$, $F = 5$, and $\Omega_p = 2$. Then, in compliance with (7), the periodic solution of (4) has the form:

$$a(t) = 10e^{-2it}, \tag{9}$$

and in the phase space it satisfies the following equation:

$$(\mathrm{Re}\, a)^2 + (\mathrm{Im}\, a)^2 = 100. \tag{10}$$

As a result, for the initial condition $a_0 = 10$, the phase point draws simply a circle described by (10). But if the system (4) starts from another initial condition, we observe the following interesting behavior: after some time, the phase point tends to one of the two orbits: $(\mathrm{Re}\, a)^2 + (\mathrm{Im}\, a)^2 = 100$ or $(\mathrm{Re}\, a)^2 + (\mathrm{Im}\, a)^2 = 50$. Two examples of such behavior of the phase point are illustrated in Fig. 1. In Fig. 1(a), the phase point (marked in pink) starts from the initial condition $\mathrm{Re}\, a = 2$, $\mathrm{Im}\, a = 0$, and after the time $t = 50$ goes into the orbit of the radius $r = \sqrt{50}$. However, in Fig. 1(b), we can see how the phase point starting from the initial condition $\mathrm{Re}\, a = 10$, $\mathrm{Im}\, a = 15$ goes into the orbit of the radius $r = 10$, described by (10). It should be emphasized that the orbit $r = \sqrt{50}$ is also periodic but it does not fulfill conditions (A) and (B).

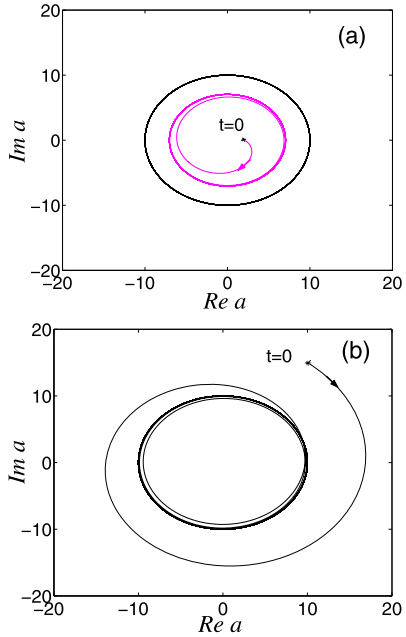

Fig. 1 The phase trajectories of the system (4) for $\omega = 1$, $\gamma = 0.5$, $\epsilon = 0.01$, $F = 5$, and $\Omega_p = 2$ and for the initial conditions: (**a**) $\mathrm{Re}\, a = 2$, $\mathrm{Im}\, a = 0$; (**b**) $\mathrm{Re}\, a = 10$, $\mathrm{Im}\, a = 15$

The solutions for this orbit has the analytical form: $(5 + 5i)\exp(-2it)$.

Both orbits: $(\mathrm{Re}\, a)^2 + (\mathrm{Im}\, a)^2 = 100$ and $(\mathrm{Re}\, a)^2 + (\mathrm{Im}\, a)^2 = 50$ are attractors of the system (4). It means that for the parameters: $\omega = 1$, $\gamma = 0.5$, $\epsilon = 0.01$, $F = 5$, and $\Omega_p = 2$ the system (4) tends to one of the two steady states (periodic), represented by these two orbits. It is easy to show that the orbit described by equation $(\mathrm{Re}\, a)^2 + (\mathrm{Im}\, a)^2 = 50$ is identical to that generated by (4) in the resonant case if $\omega = 1$, $\gamma = 0.5$, $\epsilon = 0.01$, $F = 5$, and $\Omega_p = 1$ and for the initial condition: $\mathrm{Re}\, a = 5$, $\mathrm{Im}\, a = -5$. This solution has the form: $a(t) = (5 - 5i)\exp(-it)$.

2.3 Basin of attraction

To illustrate the full influence of the initial conditions on the evolution of the system, we used the so-called *basins of attraction*. Basin of attraction is the set of initial conditions which lead to the system's attractor. The basins of attraction of the system (4) for $\omega = 1$, $\gamma = 0.5$, $\epsilon = 0.01$, $F = 5$, and $\Omega_p = 2$ are presented in Fig. 2. There are two attractors of the system (limit cycles $r = 10$ and $r' = \sqrt{50}$) and their basins of attraction are marked by different colors; the yellow area marks the basin of attraction of the attractor $(\mathrm{Re}\, a_1)^2 + (\mathrm{Im}\, a_1)^2 = 100$, whereas the blue one refers to the basin of attraction of the attractor $(\mathrm{Re}\, a_1)^2 + (\mathrm{Im}\, a_1)^2 = 50$. Both basins have interesting geometries. The basin corresponding to the circle of the radius $r' = \sqrt{50}$ has a spiral-like form with the slip and width decreasing when moving away from the

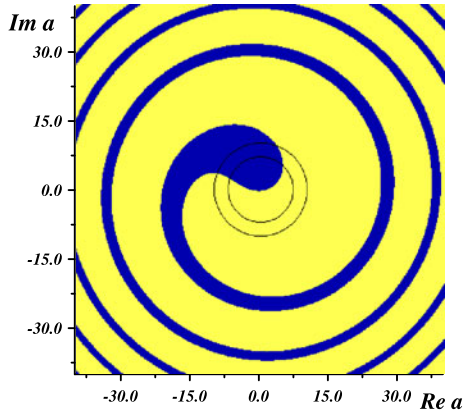

Fig. 2 Basins of attraction for two attractors—limit cycles for $r = 10$ and $r' = \sqrt{50}$. The parameters of the system (7) are: $\omega = 1$, $\gamma = 0.5$, $\epsilon = 0.01$, $F = 5$ and $\Omega_p = 2$

centre. The remaining area (blue color) refers to the basin of attraction of the second attractor (the circle of the radius $r = 10$). Both attractors have a special property. They are localized in such a way that each attractor is located partly in its own basin of attraction and partly in the basin of attraction of the other attractor. As a result—if the phase point starts from the part of the attractor situated in the basin of attraction of the other one, it escapes to the other attractor. However, if it starts from the part of the attractor situated in its own basin of attraction, it does not change the attractor. In analogy to semistable orbits, these attractors can be called the *semistable attractors*. So, the system with Kerr nonlinearity is tunable: an adequate choice of the initial condition can result in the transition of the phase point from the one attractor to the other. This property seems to be useful in applications in optical switches.

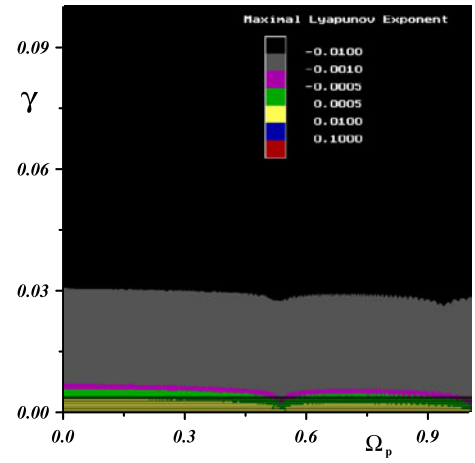

Fig. 3 Lyapunov map—the values of the maximal Lyapunov exponent λ_1 for the parameters of the system (11): $\omega = 1$, $\epsilon = 0.01$ and for the pump field amplitude $F = 5$. The initial condition is: $\mathrm{Re}\, a = 10$, $\mathrm{Im}\, a = 0$. In the parameter space (Ω_p, γ), the colors correspond to appropriate values of λ_1

2.4 Parameters detuning

One of the important properties of dynamical systems is their sensitivity to the change in the system's parameters. A small change in a parameter can lead to radical changes in the dynamics of the system. This feature is frequently used to control the dynamical systems. Globally, the behavior of the system can be shown on the so-called Lyapunov map in a parametric space. We used here the well-known procedure[13] for numerical calculation of Lyapunov exponents (Lyapunov spectrum $\lambda_i, i = 1, 2$). In Fig. 3, we show the map of maximal Lyapunov exponent λ_1 for the parameters of the system $\omega = 1$, $\epsilon = 0.01$, and for the pump field amplitude $F = 5$. The map is presented in the parameters space (Ω_p, γ). The highest values of λ_1 corresponding to chaotic oscillations are marked by red and blue colors. The chaotic motion exists only for weak damping. For higher damping constants, we find only single islands of chaotic motion in the pump field parametric space (Ω_p, F) (see Fig. 4).

To control our system of Kerr oscillators, we first change the value of one of the parameters (γ, F, or Ω_p) of the system (4) at time t_1. In such a way, the phase point being in one of the two orbits (attractors) shown in Fig. 2 escapes from the attractor to the transient state and sometimes to the new periodic state. Then after returning at time $t_2 > t_1$ to the initial values of this parameter, the additional periodic state disappears and the phase point trajectory tends to one of the two attractors of the system, depending on which basin of attraction was the phase point at time t_2. So, through the appropriate choices of times t_1 end t_2 as well as the values of the parameters of the system, we can control its evolution. In particular, we can switch the system between two stable periodic states. Such situations are illustrated in Fig. 5(a)–(c). In Fig. 5(a), the phase point starting from the orbit of the radius $r = 10$ (marked in red) after detuning the value of the damping constant γ in time $t_1 = 20$ from $\gamma = 0.5$ to $\gamma = 0.02$ escapes through a transient state to the new periodic state $r = 11.91$. After coming back with γ to the initial value $\gamma = 0.5$, it goes into the initial orbit (of the radius $r = 10$). In Fig. 5(b), the phase point starts also from the point lying on the orbit of the radius $r = 10$ and after detuning the parameter Ω_p from $\Omega_p = 2$ to $\Omega_p = 4$ at time $t_1 = 20$ it escapes through a transient state to the new periodic state $r = 1.84$. Then after coming back with the parameter Ω_p at time $t_2 = 40$ to the initial value $\Omega_p = 2$ it goes into the orbit of the radius $r' = \sqrt{50}$—the case of switching between the periodic orbits. Moreover, Fig. 5(c) shows the phase point starting from the site lying on the orbit of the radius $r = 10$ after detuning the value of the parameter F from $F = 5$ to $F = 2$ at time $t_1 = 20$ also moves to another periodic orbit $r = 1.84$, and then after returning at time $t_2 = 40$ to the initial value of parameter F ($F = 5$) it goes into the orbit of the radius $r' = \sqrt{50}$. Generally, it is very interesting that if we

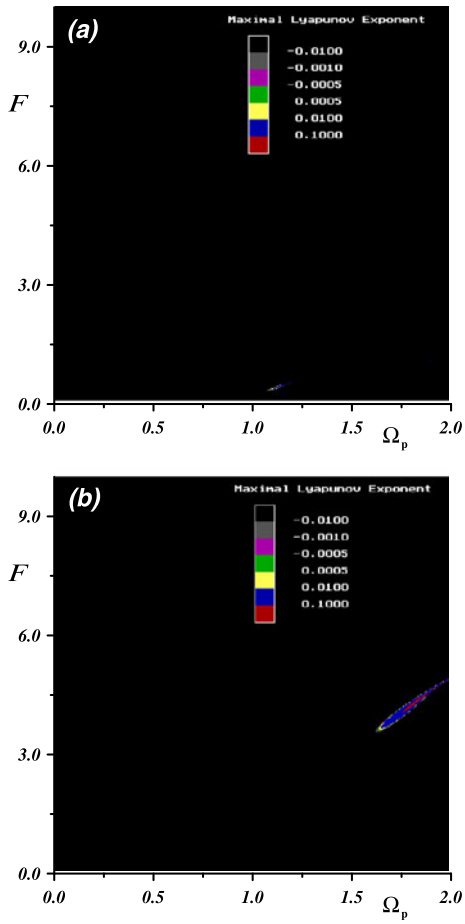

Fig. 4 Lyapunov maps—the values of the maximal Lyapunov exponent λ_1 for the parameters of the system (11): $\omega = 1$, $\epsilon = 0.01$, and for the initial condition: $\mathrm{Re}\, a = 10$, $\mathrm{Im}\, a = 0$. The parameter spaces (Ω_p, F) are presented for (**a**) $\gamma = 0.1$ and (**b**) $\gamma = 0.5$. For higher values of γ, only the periodic behavior of the system is observed

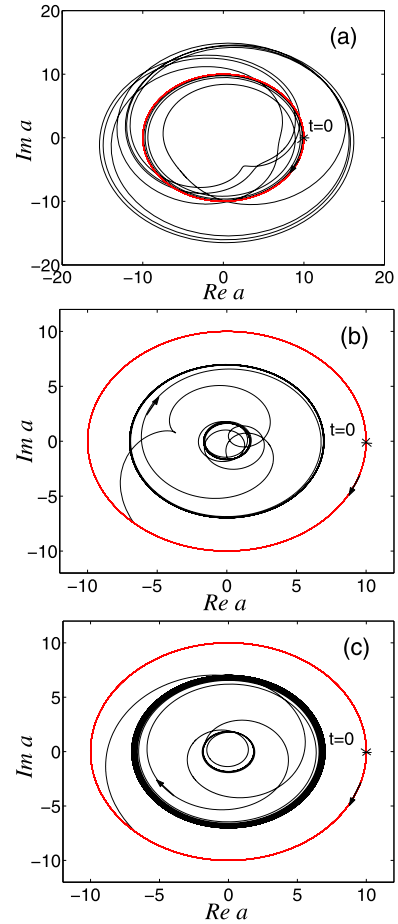

Fig. 5 The phase trajectories of the system (5) for the initial conditions: $\mathrm{Re}\, a = 10$, $\mathrm{Im}\, a = 0$ and for the following values of the system's parameters: (**a**) $\omega = 1$, $\epsilon = 0.01$, $F = 5$, $\Omega_p = 2$, and $\gamma = 0.5$ for $0 < t < 20$, $\gamma = 0.02$ for $20 < t < 40$ and $\gamma = 0.5$ for $40 < t < 60$; (**b**) $\omega = 1$, $\gamma = 0.5$, $\epsilon = 0.01$, $F = 5$, and $\Omega_p = 2$ for $0 < t < 20$, $\Omega_p = 4$ for $20 < t < 40$ and $\Omega_p = 2$ for $40 < t < 100$; (**c**) $\omega = 1$, $\gamma = 0.5$, $\epsilon = 0.01$, $\Omega_p = 2$, and $F = 5$ for $0 < t < 20$, $F = 2$ for $20 < t < 40$ and $F = 5$ for $40 < t < 250$

change the parameters of the system, some extra periodic orbits appear.

2.5 Generation of chaotic beats

Since the publication of [14], the new type of signals called "chaotic beats" has been investigated [15] and experimentally generated [16–19]. There are two basic kinds of chaotic beats: (1) the signals with chaotic envelopes and a stable fundamental frequency, and (2) the signals with almost regular collapses and revivals with small chaotic perturbations. Generally, when the system is subjected to an external field, we can generate the chaotic beats in two ways by modulation of the amplitude or frequency of the external field.

The more effective method of generation of chaotic beats in system (4) seems to be the frequency modulation, according to the formula:

$$\Omega_p \to \Omega_p(1 + \Delta\Omega_p \sin(\mu t)),$$

where μ is the frequency of modulation parameter, and $\Delta\Omega_p$ is the amplitude of this modulation. Then the

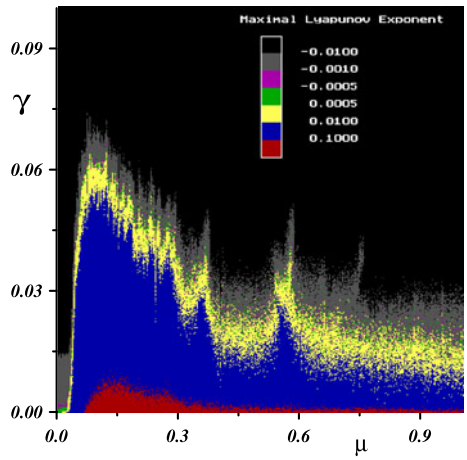

Fig. 6 The values of maximal Lyapunov exponent λ_1 for the system (11) as a function of the damping parameter γ and the frequency modulation μ, for $\epsilon = 0.01$, $F = 5$, $\Omega_p = 2$, and with the initial condition: $\mathrm{Re}\, a = 10$, $\mathrm{Im}\, a = 0$

equation of motion for variable a takes the form:

$$\frac{da}{dt} = -i\omega a - i\epsilon a^* a^2 - \gamma a + F e^{-i\Omega_p(1+\Delta\Omega_p \sin(\mu t))t}. \tag{11}$$

In numerical calculations, we put $\Delta\Omega_p = 0.1$.

The global dynamics of system (11) is presented in Fig. 6 as a Lyapunov map in the parametric space of (γ, μ), where the values of the first Lyapunov exponent λ_1 are marked by appropriate colors. The highest values of λ_1 corresponding to chaotic oscillations are marked by red and blue colors. As we can see, they are concentrated in the lower part of the map which corresponds to the low values of the damping parameter γ (mainly for $\gamma < 0.05$). For higher γ, the map is dominated by the black and grey colors corresponding to the periodic states. An example of chaotic beats generated in the system (11) through frequency modulation (with $\gamma = 0.02$ and $\mu = 0.15$) is presented in Fig. 7. The spectrum of the Lyapunov exponents $\{0.0519, -0.0813\}$ of that system with the positive value of λ_1 indicates chaotic behavior.

Similar results were obtained for the resonance case ($\Omega_p = \omega$). The values of maximal Lyapunov exponent λ_1 for system (11) as a function of the damping parameter γ ($0 < \gamma < 0.5$) and the frequency modulation μ ($0 < \mu < 1$) and for $\Omega_p = \omega = 1$ are presented in Fig. 8.

Analogically as for the nonresonance case, the chaotic behavior is obtained only for the low values

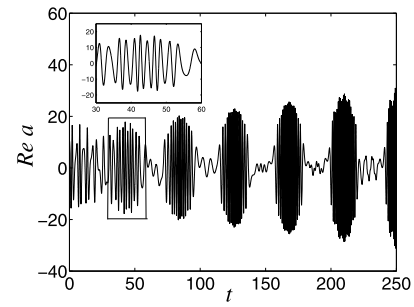

Fig. 7 Time dependence of $\mathrm{Re}\, a$ of the system (11), for $\gamma = 0.02$ and $\mu = 0.15$. The other parameters are: $\omega = 1$, $F = 5$, $\epsilon = 0.01$ and $\Omega_p = 2$. The system starts from the initial condition: $\mathrm{Re}\, a = 10$, $\mathrm{Im}\, a = 0$. Chaotic beats

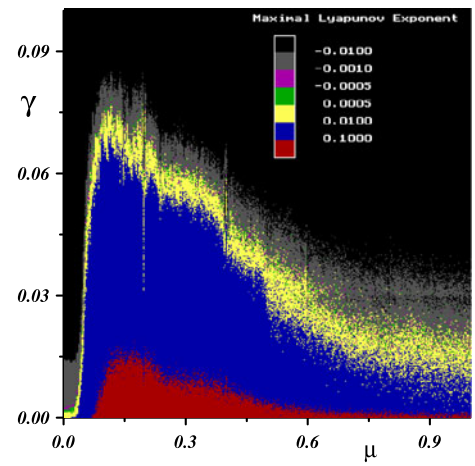

Fig. 8 The values of the maximal Lyapunov exponent λ_1 of system (11) as a function of the damping parameter γ and the frequency of modulation μ, for $\epsilon = 0.01$, $F = 5$ and $\Omega_p = \omega = 1$ (the resonant case) and with the initial conditions: $\mathrm{Re}\, a = 10$, $\mathrm{Im}\, a = 0$

of the damping parameter γ (mainly for $\gamma < 0.05$). In Fig. 9, we can see the time dependence of $\mathrm{Re}\, a$ of the system (11), for $\gamma = 0.01$, $\mu = 0.15$, and $\Omega_p = \omega = 1$.

The spectrum of Lyapunov exponents of the beats shown in Fig. 9 is $\{0.1085, -0.1230\}$ and contains positive value of λ_1 indicating chaotic behavior.

3 The two coupled Kerr oscillators

3.1 Equations of motion

It is interesting to know what happens to the dynamics of the single Kerr oscillator after coupling it nonlinearly to another analogous oscillator but of different

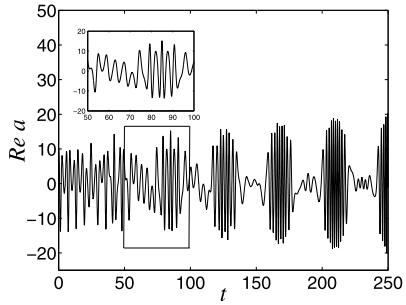

Fig. 9 Time dependence of $\mathrm{Re}\,a$ of system (11), for $\gamma = 0.01$, $\mu = 0.15$, $F = 5$, $\epsilon = 0.01$, and $\Omega_p = \omega = 1$. The system starts from the initial condition: $\mathrm{Re}\,a = 10$, $\mathrm{Im}\,a = 0$. Chaotic beats

frequency. Such a system of two nonlinearly coupled Kerr oscillators (nonlinear couplers) is described by the following Hamiltonian:

$$H = H_0 + H_1 + H_2, \tag{12}$$

where:

$$H_0 = \sum_{j=1}^{2} \omega_j a_j^* a_j + \frac{1}{2} \sum_{j=1}^{2} \epsilon_j a_j^{*2} a_j^2, \tag{13}$$

$$H_1 = \epsilon_{12} a_1^* a_2^* a_1 a_2, \tag{14}$$

$$H_2 = i \sum_{j=1}^{2} \left[F_j \left(a_j^* e^{-i\Omega_{jp} t} - a_j e^{i\Omega_{jp} t} \right) \right]. \tag{15}$$

The Hamiltonian H_0 represents the two single Kerr oscillators, H_1 is the Hamiltonian of the interaction between them and H_2 describes the interaction of the two oscillators with the external fields. The values a_1 and a_2 are complex dynamical variables, ω_j denote the frequencies of the free vibrations of the two single oscillators; ϵ_1 and ϵ_2 are Kerr parameters describing nonlinearity in these subsystems (oscillators) and ϵ_{12} is the parameter of nonlinear coupling between them.

The equations of motion for variables a_1 and a_2 have the form:

$$\frac{da_1}{dt} = -i\omega_1 a_1 - i\epsilon_1 a_1^* a_1^2 - i\epsilon_{12} a_2^* a_1 a_2 + F_1 e^{-i\Omega_{1p} t} - \gamma_1 a_1, \tag{16}$$

$$\frac{da_2}{dt} = -i\omega_2 a_2 - i\epsilon_2 a_2^* a_2^2 - i\epsilon_{12} a_1^* a_1 a_2 + F_2 e^{-i\Omega_{2p} t} - \gamma_2 a_2, \tag{17}$$

where the terms $\gamma_1 a_1$ and $\gamma_2 a_2$, describing the dissipation of energy, with damping constants γ_1 and γ_2, are added to the equations of motion on phenomenological grounds. In the autonomous and conservative case, that is when $\gamma_1 = \gamma_2 = F_1 = F_2 = 0$ the solutions of (16)–(17) have the form:

$$a_1(t) = a_{10} e^{-i(\omega_1 + \epsilon_1 a_{10}^* a_{10} + \epsilon_{12} a_{20}^* a_{20})t}, \tag{18}$$

$$a_2(t) = a_{20} e^{-i(\omega_2 + \epsilon_2 a_{20}^* a_{20} + \epsilon_{12} a_{10}^* a_{10})t}, \tag{19}$$

where $a_1(t)\,|_{t=0} \equiv a_{10}$ and $a_2(t)\,|_{t=0} \equiv a_{20}$ denote initial conditions.

In the nonautonomous case (16)–(17), we find periodic solutions in the form of the following functions (in analogy to the case of the single Kerr oscillator):

$$a_1(t) = x_1 e^{-i(\omega_1 + \epsilon_1 x_1^* x_1 + \epsilon_{12} x_2^* x_2)t}, \tag{20}$$

$$a_2(t) = x_2 e^{-i(\omega_2 + \epsilon_2 x_2^* x_2 + \epsilon_{12} x_1^* x_1)t}, \tag{21}$$

that is in the form of the solutions of the autonomous one. Functions (20)–(21) satisfy the equations of motion (16)–(17) on condition that $x_j = F_j/\gamma_j$, $j = 1, 2$. As a result, these solutions have the form:

$$a_1(t) = \frac{F_1}{\gamma_1} \exp\left[-i \left(\omega_1 + \epsilon_1 \frac{F_1^2}{\gamma_1^2} + \epsilon_{12} \frac{F_2^2}{\gamma_2^2} \right) t \right], \tag{22}$$

$$a_2(t) = \frac{F_2}{\gamma_2} \exp\left[-i \left(\omega_2 + \epsilon_2 \frac{F_2^2}{\gamma_2^2} + \epsilon_{12} \frac{F_1^2}{\gamma_1^2} \right) t \right]. \tag{23}$$

Then $\Omega_{1p} = \omega_1 + \epsilon_1 F_1^2/\gamma_1^2 + \epsilon_{12} F_2^2/\gamma_2^2$ and $\Omega_{2p} = \omega_2 + \epsilon_2 F_2^2/\gamma_2^2 + \epsilon_{12} F_1^2/\gamma_1^2$.

In the phase plane ($\mathrm{Re}\,a_1$, $\mathrm{Im}\,a_1$, $\mathrm{Re}\,a_2$, $\mathrm{Im}\,a_2$), the periodic solutions (22)–(23) satisfy the phase equations (limit cycles–circles):

$$(\mathrm{Re}\,a_j)^2 + (\mathrm{Im}\,a_j)^2 = \frac{F_j^2}{\gamma_j^2}, \quad \text{where } j = 1, 2, \tag{24}$$

for any values of frequencies ω_1, ω_2.

3.2 The dynamics of the system in the phase space

Coupling the single Kerr oscillator described by (4) to the other analogous oscillator but with different own frequency causes distinct changes in its dynamics, as illustrated by the diagrams in the phase space.

Let us consider two nonlinearly coupled Kerr oscillators (subsystems) described by (16)–(17) if $\omega_1 = 1$, $\omega_2 = 0.5$, $\epsilon_1 = \epsilon_2 = 0.01$, $F_1 = F_2 = 5$, $\gamma_1 = \gamma_2 = 0.5$, $\Omega_{1p} = 3.0$, $\Omega_{2p} = 2.5$, and $\epsilon_{12} = 0.01$. Then, in

compliance with (22)–(23), the periodic solutions of (16)–(17) have the form:

$$a_1(t) = 10e^{-3.0it}, \tag{25}$$

$$a_2(t) = 10e^{-2.5it}, \tag{26}$$

and in the phase space they satisfy the following equations:

$$(\mathrm{Re}\, a_1)^2 + (\mathrm{Im}\, a_1)^2 = 100, \tag{27}$$

$$(\mathrm{Re}\, a_2)^2 + (\mathrm{Im}\, a_2)^2 = 100. \tag{28}$$

As a result, for the initial conditions $a_{10} = 10$ and $a_{20} = 10$, the phase points of both subsystems draw the same circle of the radius $r = 10$ described by (27)–(28), with frequencies $\Omega_{1p} = 3.0$ and $\Omega_{2p} = 2.5$, respectively. But if the phase point representing the first subsystem (at frequency $\omega_1 = 1$) starts from another initial condition instead of $a_{10} = 10$, and a_{20} is fixed ($a_{20} = 10$), the following behavior is observed: the phase point representing the first subsystem after some time tends to one of the two orbits being attractors of subsystem (16): $(\mathrm{Re}\, a_1)^2 + (\mathrm{Im}\, a_1)^2 = 100$ or $(\mathrm{Re}\, a_1)^2 + (\mathrm{Im}\, a_1)^2 = 6.6987$. The second orbit belongs to the periodic solution: $a_1(t) = (10/(1 - i(2 - \sqrt{3}))\exp(-3.0it)$ and $a_2(t) = (10/(1 - i(2 - \sqrt{3}))\exp(-2.5it)$. This situation is illustrated in Fig. 10. In Fig. 10(a), the phase point representing the first subsystem starts from the initial condition $\mathrm{Re}\, a_{10} = 0$, $\mathrm{Im}\, a_{10} = 15$ (the initial condition for the second subsystem (17) is fixed: $\mathrm{Re}\, a_{20} = 10$, $\mathrm{Im}\, a_{20} = 0$) and after the time $t = 50$ it goes into the attractor of the radius $r = 10$, described by (27). However, Fig. 10(b) shows the phase point starting from the initial condition $\mathrm{Re}\, a_{10} = 0$, $\mathrm{Im}\, a_{10} = 7$ and going into the orbit of the radius $r' = \sqrt{6.6987}$.

The third solution of (16) and (17) is completely unstable and has the form: $a_1(t) = (10/(1 - i(2 + \sqrt{3}))\exp(-3.0it)$ and $a_2(t) = (10/(1 - i(2 + \sqrt{3}))\exp(-2.5it)$.

3.3 Basins of attraction

Figure 11 shows two attractors and their basins of attraction of subsystem (16) marked by appropriate colors; the initial condition of subsystem (17) is fixed ($a_{20} = 10$). The yellow area marks the basin of attraction of the attractor of the radius $r = 10$, whereas the blue one corresponds to the basin of attraction of the attractor of the radius $r' = \sqrt{6.6987}$. The basin marked in yellow has a special geometry: it consists of two separate areas, one of which has a spiral-like form. Both, the slip of the spiral and its width decrease

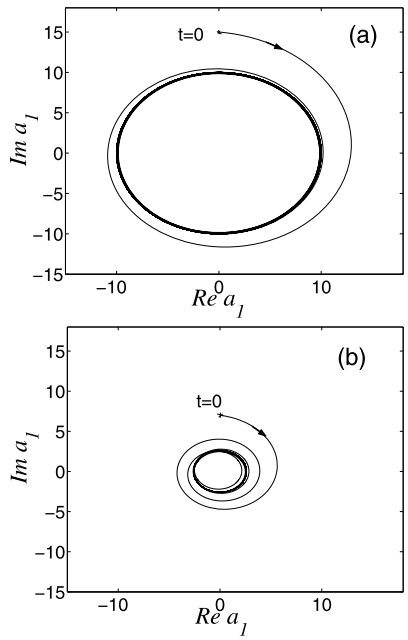

Fig. 10 The phase trajectories of subsystem (16) if $\omega_1 = 1$, $\omega_2 = 0.5$, $\epsilon_1 = \epsilon_2 = 0.01$, $F_1 = F_2 = 5$, $\gamma_1 = \gamma_2 = 0.5$, $\Omega_{1p} = 3.0$, $\Omega_{2p} = 2.5$, $\epsilon_{12} = 0.01$, and for the initial conditions: (**a**) $\mathrm{Re}\, a_{10} = 0$, $\mathrm{Im}\, a_{10} = 15$, $\mathrm{Re}\, a_{20} = 10$, $\mathrm{Im}\, a_{20} = 0$; (**b**) $\mathrm{Re}\, a_{10} = 0$, $\mathrm{Im}\, a_{10} = 7$, $\mathrm{Re}\, a_{20} = 10$, $\mathrm{Im}\, a_{20} = 0$

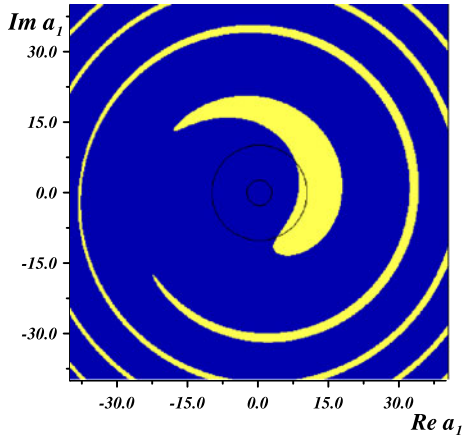

Fig. 11 Basins of attraction of two coupled Kerr oscillators. The parameters of the systems are: $\omega_1 = 1$, $\omega_2 = 0.5$, $\epsilon_1 = \epsilon_2 = 0.01$, $F_1 = F_2 = 5$, $\gamma_1 = \gamma_2 = 0.5$, $\Omega_{1p} = 3.0$, $\Omega_{2p} = 2.5$, $\epsilon_{12} = 0.01$, and the initial conditions are: $\mathrm{Re}\, a_{10} = 0$, $\mathrm{Im}\, a_{10} = 15$, $\mathrm{Re}\, a_{20} = 10$, $\mathrm{Im}\, a_{20} = 0$. Stable ($r' = \sqrt{6.6987}$) and semistable ($r = 10$) attractors

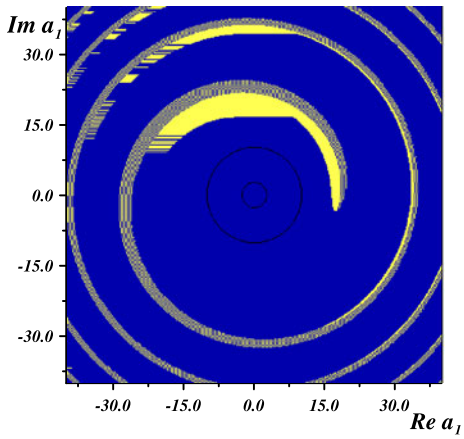

Fig. 12 Basins of attraction of two coupled Kerr oscillators. The parameters are the same as in Fig. 11, but $\mathrm{Re}\, a_{20} = 0$, $\mathrm{Im}\, a_{20} = 0$. Stable ($r' = \sqrt{6.6987}$) and unstable ($r = 10$) attractors

toward moving away from the center, similarly, as for the single Kerr oscillator. Contrary to the case of the single Kerr oscillator there is an island in the central part of the basin. The remaining area (blue color) is the basin of attraction of the other attractor (the circle of the radius $r' = \sqrt{6.6987}$).

The attractor of the radius $r' = \sqrt{6.6987}$ is stable (it is fully in its own basin of attraction), however, the attractor of the radius $r = 10$ is semistable (it is partly in its own basin of attraction and partly in the basin of attraction of the other attractor). As a result, the transition from the attractor of the radius $r = 10$ to the attractor of the radius $r' = \sqrt{6.6987}$ is possible, but that in opposite direction is impossible, because the phase point starting from any position on the circle $(\mathrm{Re}\, a)^2 + (\mathrm{Im}\, a)^2 = 6.6987$ always returns to it.

The types of attractors change after changing the initial condition of the subsystem (17). For example, Fig. 12 shows the attractors and their basins of attractions of subsystem (16) for $a_{20} = 0$. The basin of attraction corresponding to the circle of the radius $r = 10$ is marked by yellow; the remaining area (blue color) refers to the basin of attraction of the circle of $r' = \sqrt{6.6987}$. As we can see, in this case the attractor with radii ($r' = \sqrt{6.6987}$) is stable, and the other one is completely unstable.

3.4 Generation of chaotic beats

Globally, the behavior of system (16)–(17) is presented in Fig. 13(a) showing the Lyapunov map in the parameters space (ϵ_{12}, γ). We find that strong chaotic behavior of the system is much common that for the single Kerr system. We also notice that if we increase the dumping in the system we must increase the coupling between subsystems to achieve the chaotic behavior. The full spectrum of the Lyapunov exponents $\{\lambda_1, \lambda_2, \lambda_3, \lambda_4\}$ versus ϵ_{12} shows the regions of order or chaos in the cross section of the map for the damping parameter $\gamma = \gamma_1 = \gamma_2 = 0.5$ (Fig. 13(b)). If $\lambda_1 > 0$, then the system is chaotic, and if $\lambda_1 \leq 0$, it behaves periodically. The system with the parameters of Fig. 13 and for the coupling constant $\epsilon_{12} > 1.6$ manifests extremely unstable behavior and its solutions are divergent to infinity. There is also a region of hyperchaotic behavior of the system in which two highest Lyapunov exponents are positive (for $\epsilon_{12} > 0.44$).

Taking from Fig. 13(a)–(b), the appropriate values of the damping constant $\gamma_1 = \gamma_2 = 0.5$ and the nonlinear coupling between the Kerr oscillators $\epsilon_{12} = 0.45$ we can generate chaotic beats in the system of two nonlinearly coupled Kerr oscillators (16)–(17), both being initially in the periodic state. Such chaotic beats are shown in Fig. 14 illustrating the time dependence of $\mathrm{Re}\, a_1$ and $\mathrm{Re}\, a_2$. Because the spectrum of Lyapunov exponents of the beats shown in Fig. 14 is

$$\{0.0708, 0.0205, -1.4552, -1.5215\}$$

and contains two positive values we can even call it hyperchaotic beats [20].

4 Conclusion

The Kerr effect and the Kerr couplers considered in this paper have great potential in studies and applications of optical devices like optical fibers or couplers. From this point of view, the main results of this paper are: (1) Tunneling properties of periodic attractors (mutual interpenetration of attractors and basins of attraction) lead to the possibility of switching of Kerr oscillator system between different semistable attractors by changing initial condition (Sect. 2.3). (2) As shown in Sect. 2.4, the dynamics of the Kerr system can be controlled by appropriate switching of the parameters of the system or the external field. Temporary changes in parameters also switch the system between different periodic states. (3) The system with Kerr nonlinearity is able to generate chaotic

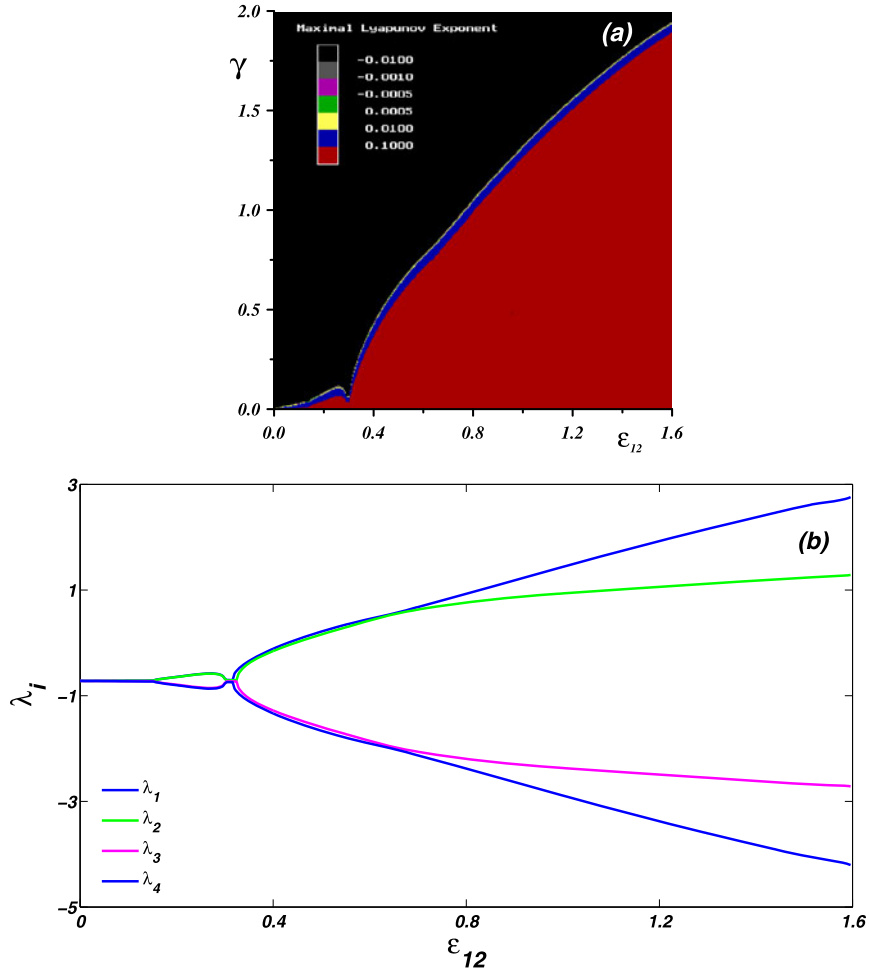

Fig. 13 (**a**) The Lyapunov map of the system (16)–(17) in the parametric space (ϵ_{12}, γ) where $\gamma = \gamma_1 = \gamma_2$. (**b**) The full spectrum of Lyapunov exponents $\{\lambda_1, \lambda_2, \lambda_3, \lambda_4\}$ of the system (16)–(17) as a function of the nonlinear coupling parameter ϵ_{12} and for $\gamma = \gamma_1 = \gamma_2 = 0.5$. The rest of parameters for both figures are: $\omega_1 = 1$, $\omega_2 = 0.5$, $\epsilon_1 = \epsilon_2 = 0.01$, $F_1 = F_2 = 5$, $\Omega_{1p} = 3$ and $\Omega_{2p} = 2.5$. The system starts from the initial conditions: $\mathrm{Re}\, a_1 = 10$, $\mathrm{Im}\, a_1 = 0$, $\mathrm{Re}\, a_2 = 10$, $\mathrm{Im}\, a_2 = 0$

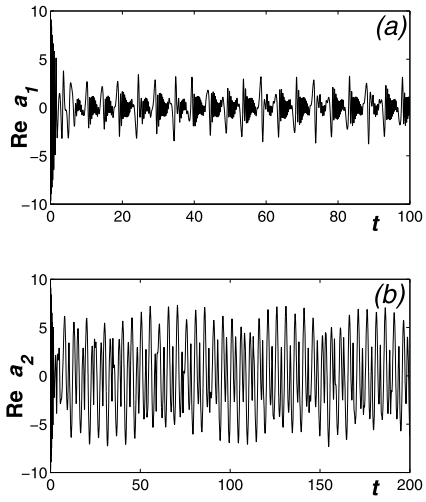

Fig. 14 Time dependence of $\mathrm{Re}\, a_1$ (**a**) and $\mathrm{Re}\, a_2$ (**b**) of the system (16)–(17). Parameters are the same as in Fig. 13(b), and $\epsilon_{12} = 0.45$. Chaotic beats

beats (Sect. 2.5). The properties of these beats depend on specific choices of parameters of the system and the external field. (4) For two coupled Kerr oscillators, it is possible to change the stability of attractors of a given subsystem by changing the initial conditions of the other subsystem and the dynamics of one subsystem can be controlled by changing the initial conditions of the other one (Sect. 3.3). (5) Moreover, chaotic (or hyperchaotic) beats in the system of two coupled Kerr oscillators can be generated (Sect. 3.4).

References

1. Milburn, G.J., Holmes, C.A.: Quantum coherence and classical chaos in a pulsed parametric oscillator with a Kerr nonlinearity. Phys. Rev. A **44**, 4704–4711 (1991)
2. Wielinga, B., Milburn, G.J.: Chaos and coherence in an optical system subject to photon nondemolition measurement. Phys. Rev. A **46**, 762–770 (1992)
3. Szlachetka, P., Grygiel, K., Bajer, J.: Chaos and order in a kicked anharmonic oscillator: classical and quantum analysis. Phys. Rev. E **48**, 101–108 (1993)
4. Leoński, W., Tanaś, R.: Possibility of producing the one-photon state in a kicked cavity with a nonlinear Kerr medium. Phys. Rev. A **49**, R20–R23 (1994)
5. Kowalewska-Kudlaszyk, A., Kalaga, J.K., Leoński, W.: Long-time fidelity and chaos for a kicked nonlinear oscillator system. Phys. Lett. A **373**, 1334–1340 (2009)
6. Jensen, S.M.: Nonlinear coherent coupler. IEEE J. Quantum Electron. **QE-18**, 1580–1583 (1982)
7. Kenkre, V.M., Campbell, D.K.: Self-trapping on a dimer: time-dependent solutions of a discrete nonlinear Schrödinger equation. Phys. Rev. B **34**, 4959–4961 (1986)
8. Chefles, A., Barnet, S.M.: Quantum theory of two-mode nonlinear directional couplers. J. Mod. Opt. **43**, 709–727 (1996)
9. Fiurasek, J., Krepelka, J., Perina, J.: Quantum-phase properties of the Kerr couplers. Opt. Commun. **167**, 115–124 (1999)
10. Pecora, L.M., Caroll, T.L.: Synchronization in chaotic systems. Phys. Rev. Lett. **64**, 821–824 (1990)
11. Grygiel, K., Szlachetka, P.: Dynamics and synchronization of linearly coupled Kerr oscillators. J. Opt. B, Quantum Semiclass. Opt. **3**, 104–110 (2001)
12. Szlachetka, P., Grygiel, K., Misiak, M.: Synchronization of two low-dimensional Kerr chains. Chaos Solitons Fractals **27**, 673–684 (2006)
13. Wolf, A., Swift, J.B., Swinney, H.L., Vastano, J.A.: Determining Lyapunov exponents from a time series. Physica D **16**, 285–317 (1985)
14. Grygiel, K., Szlachetka, P.: Generation of chaotic beats. Int. J. Bif. Chaos **12**, 635–644 (2002)
15. Śliwa, I., Szlachetka, P., Grygiel, K.: Chaotic beats in a nonautonomous system governing second-harmonic generation of light. Int. J. Bif. Chaos **17**, 3253–3257 (2007)
16. Cafagna, D., Grassi, G.: A new phenomenon on nonautonomous Chua's circuits: generation of chaotic beats. Int. J. Bif. Chaos **14**, 1773–1788 (2004)
17. Cafagna, D., Grassi, G.: Chaotic beats in a modified Chua's circuits: Dynamic behavior and circuit design. Int. J. Bif. Chaos **14**, 3045–3064 (2004)
18. Cafagna, D., Grassi, G.: Generation of chaotic beats in a modified Chua's circuits—part I: dynamic behavior. Nonlinear Dyn. **44**, 91–99 (2006)
19. Cafagna, D., Grassi, G.: Generation of chaotic beats in a modified Chua's circuits—part II: circuit design. Nonlinear Dyn. **44**, 101–108 (2006)
20. Śliwa, I., Grygiel, K., Szlachetka, P.: Hyperchaotic beats and their collapse to the quasiperiodic oscillations. Nonlinear Dyn. **53**, 13–18 (2008)